Int J Earth Sci (Geol Rundsch) (2016) 105:1021–1037
DOI 10.1007/s00531-015-1212-0

ORIGINAL PAPER

Early middle Miocene tectonic uplift of the northwestern part of the Qinghai–Tibetan Plateau evidenced by geochemical and mineralogical records in the western Tarim Basin

Chaowen Wang[1,2] · Hanlie Hong[1] · Hemmo A. Abels[2] · Zhaohui Li[3,4] · Kai Cao[4] · Ke Yin[1,4] · Bowen Song[1] · Yadong Xu[1] · Junliang Ji[1] · Kexin Zhang[1,4]

Received: 29 September 2014 / Accepted: 3 June 2015 / Published online: 19 June 2015

Abstract The Tarim Basin in western China has been receiving continuous marine to lacustrine deposits during the Cenozoic as a foreland basin of the Qinghai–Tibetan Plateau (QTP). Clay mineralogy and geochemical proxy data from these sedimentary archives can shed light on climate and tectonic trends. Here we report on an abrupt mineralogical and weathering shift at 17 Ma ± 1 Myr in the Miocene Qimugan section in the northwestern part of the Qinghai–Tibetan Plateau. The rapid shift involves decreasing trends of chemical weathering indices, Rb/Sr and Ba/Sr ratios, and of minor and immobile elements with respect to upper crust composition as well as increasing trends of Na/Al and Na/Ti ratios, smectite, chlorite, and calcite contents. We ascribe these trends to changing source rocks due to uplift of the northern part of the QTP leading to exposures of younger intrusive bodies and older gneisses, schists, and carbonate-rich rocks. These uplifts potentially caused regional aridification reducing chemical weathering. The dating is indirect via magnetostratigraphically dated ostracod biostratigraphy and detrital zircon chronology and currently not good enough to compare the shift accurately in time with the onset of the global middle Miocene Climate Optimum (MMCO) at 16.5 Ma. Nevertheless, regional tectonics seem to have dominated over global climate as the warmer MMCO is expected to have increased weathering indices and decreased Na/Al and Na/Ti, rather than the observed reverse trends.

Keywords Tarim Basin · Paleoclimate · Tectonics · Clay minerals · Qinghai–Tibetan Plateau · Chemical weathering

✉ Chaowen Wang
cwwang_cug@aliyun.com

[1] State Key Laboratory of Biogeology and Environmental Geology, China University of Geosciences, Wuhan 430074, Hubei, People's Republic of China

[2] Stratigraphy/Paleontology, Department of Earth Sciences, Utrecht University, Utrecht 3808 TA, The Netherlands

[3] Geosciences Department, University of Wisconsin - Parkside, Kenosha, WI 53141-2000, USA

[4] Faculty of Earth Sciences, China University of Geosciences, Wuhan 430074, People's Republic of China

Introduction

The Qinghai–Tibetan Plateau (QTP) has undergone a complex tectonic and climatic evolution since the collision of India with southern Eurasia in the early Cenozoic (Harrison et al. 1992; Molnar et al. 1993, 2010; Molnar and Tapponnier 1975). Tectonically, the collision resulted in a large-scale crustal shortening and thickening throughout the Qinghai–Tibetan Plateau. Deformation is observed along the Himalayan orogenic belt (DeCelles et al. 2002), normal and thrust faulting occurred in central Tibet (Blisniuk et al. 2001), and large-scale strike-slip and thrust faulting in Altyn Tagh, Qilian, Kunlun (Yin et al. 2002; Yue and Liou 1999), and the Pamir (Cao et al. 2013a, b; Robinson et al. 2004, 2007; Yin and Harrison 2000). Climatically, the uplift of the QTP caused a physical obstruction affecting atmospheric circulation and distribution, which lead to dramatic inland aridification (Molnar et al. 2010). It also caused enhanced Asian monsoon activity, despite the cooling of Cenozoic global climate and retreat of the Neo-Tethys Sea (An et al. 2001; Dupont-Nivet et al. 2008; Guo et al. 2002, 2008; Ramstein et al. 1997; Sun and Wang 2005; Xiao et al. 2010). The linkages between these tectonic and climatic changes have been largely recorded in structurally controlled depressions around the Qinghai–Tibetan

Plateau, such as the Qaidam, Xining, Linxia, Girong, and Zhada basins (Dettman et al. 2003; Dupont-Nivet et al. 2008; Graham et al. 2005; Hong et al. 2007, 2010, 2012; Rieser et al. 2009). The relationship between uplift of the QTP and climate change remains scarcely documented in the Tarim Basin.

The mountains around the Tarim Basin have undergone multiple phases of uplift based on extensive and coincident exhumation records in the Pamir, Tianshan, and Kunlun (Amidon and Hynek 2010; Sobel and Dumitru 1997; Sobel et al. 2006; Jolivet et al. 2001, 2003). Amidon and Hynek (2010) attributed the first period of tectonic uplift to the northward propagation of the deformation related to the India-Eurasia collision during middle Eocene, based on apatite and zircon (U/Th)-He ages in the Pamir. The second period is associated with a renewed phase of tectonics and plateau uplift in the Pamir (Amidon and Hynek 2010; Lukens et al. 2012) and in the Tianshan during the late Oligocene to middle Miocene (Sobel and Dumitru 1997; Sobel et al. 2006; Li and Peng 2010; Heermance et al. 2008). Meanwhile, the Kunlun strike-slip fault was also active in the Miocene at around 15 Ma (Jolivet et al. 2001, 2003). Subsequently, uplift during the middle Miocene to Pliocene is documented by apatite and zircon fission track chronological, sedimentological, and structure geological data (Wang et al. 2003a, b, 2011; Cao et al. 2013a, b; Heermance et al. 2008).

To investigate a possible link between the phases of uplift and paleoclimate, multi-proxy studies were performed in the Tarim Basin. Positive shifts in both carbon and oxygen isotopes since ~15 Ma have been interpreted to document increased regional aridity (Kent-Corson et al. 2009). Integrated magnetic susceptibility, color variations, total inorganic and organic carbon contents, and grain-sized signatures have documented regionally stepwise aridification at ~7 and ~5.3 Ma, respectively (Sun et al. 2008, 2015). These interpretations are consistent with evidence from geochemical records ($CaCO_3$ and salt ions), which suggest drying of the Asian interior since ~5.7 Ma (Zhang et al. 2013). However, it is not clear whether these signals are the direct result of regional tectonic changes (i.e., uplift of the surrounding mountain ranges) or regional climate change. The two may very well be linked, especially in the Miocene, during which coincident exhumation occurred in the Pamir, Tianshan, and Kunlun mountains (Amidon and Hynek 2010; Lukens et al. 2012; Jolivet et al. 2001, 2003).

Using clay mineralogical content of the Qimugan section in the western Tarim Basin, Wang et al. (2013a) interpreted a dramatically climatic cooling in the late Eocene to Oligocene. From the same succession, Cao et al. (2014) added whole-rock major elemental analysis to address paleoclimate and tectonic changes in the Tarim Basin in the Miocene. Here, we carefully review the age control on this succession based on detailed regional correlations of fossil ostracods and foraminifers across the Tarim Basin as well as to adjacent basins, with new magnetostratigraphic age data and detrital zircon chronology as age constraints. We integrate whole-rock mineralogical, clay mineralogical, major elemental data, and add minor elemental and mineral morphological data from the Qimugan section in the Tarim Basin to enhance the understanding of environmental change and sedimentary provenance in the northwestern part of the QTP since the early Miocene.

Geological setting

The study area is located in the southwestern part of the Tarim Basin, which is in the northwestern part of the QTP (Fig. 1a). The Tarim Basin expands over an area of ~500,000 km^2 and is surrounded by the Tianshan Mountains to the north, the Pamir Plateau to the west, the West Kunlun to the south, and Altyn Tagh Mountains along its eastern margin (Fig. 1a; Cao et al. 2013a, b; Sun et al. 2005a). In the Eocene, marine sedimentation took place in the Tarim Basin. The long-term effect of India-Eurasia collision subsequently resulted in regression of the Neo-Tethys Sea and activation of the Tianshan and Altai Shan, and initiation of major boundary faults, such as the Karakorum, the Main Pamir Thrust, the Kashgar-Yecheng transfer system, and Altyn Tagh Faults (Cao et al. 2013a, b; Sobel and Dumitru 1997; Bosboom et al. 2011, 2013).

The sedimentary facies and lithostratigraphy of the Qimugan section in the Tarim Basin have been previously documented by Jin et al. (2003) and Zhang et al. (2010). They reveal a relatively complete Cenozoic sedimentary succession including the change from a marine to a continental depositional setting. In the Qimugan section, the continental beds belong to the Keziluoyi, Anjuan, Pakabulake, and Atushi Formations. The Keziluoyi Formation lies disconformably over the marine Bashibulake Formation and consists of gypsiferous mudstones and gypsum beds in its lower portions, and grayish-red, purplish-gray, and brownish-red fine sandstones, calcareous siltstones, and calcareous mudstones in its upper portions. The Anjuan Formation is characterized by grayish-green mudstones and sandstones intercalated with grayish-green to brownish-red siltstones, with several tens of meters of grayish-green, thick-bedded fine sandstones at its base. The Pakabulake Formation consists of brownish-red, gray, and polymictic mudstones interbedded with grayish-green sandstones. The Atushi Formation is composed of gray to brownish-gray polymictic conglomerates interbedded with pinkish, fine sandstones with interlayers of mudstones, siltstones, and gypsiferous mudstones.

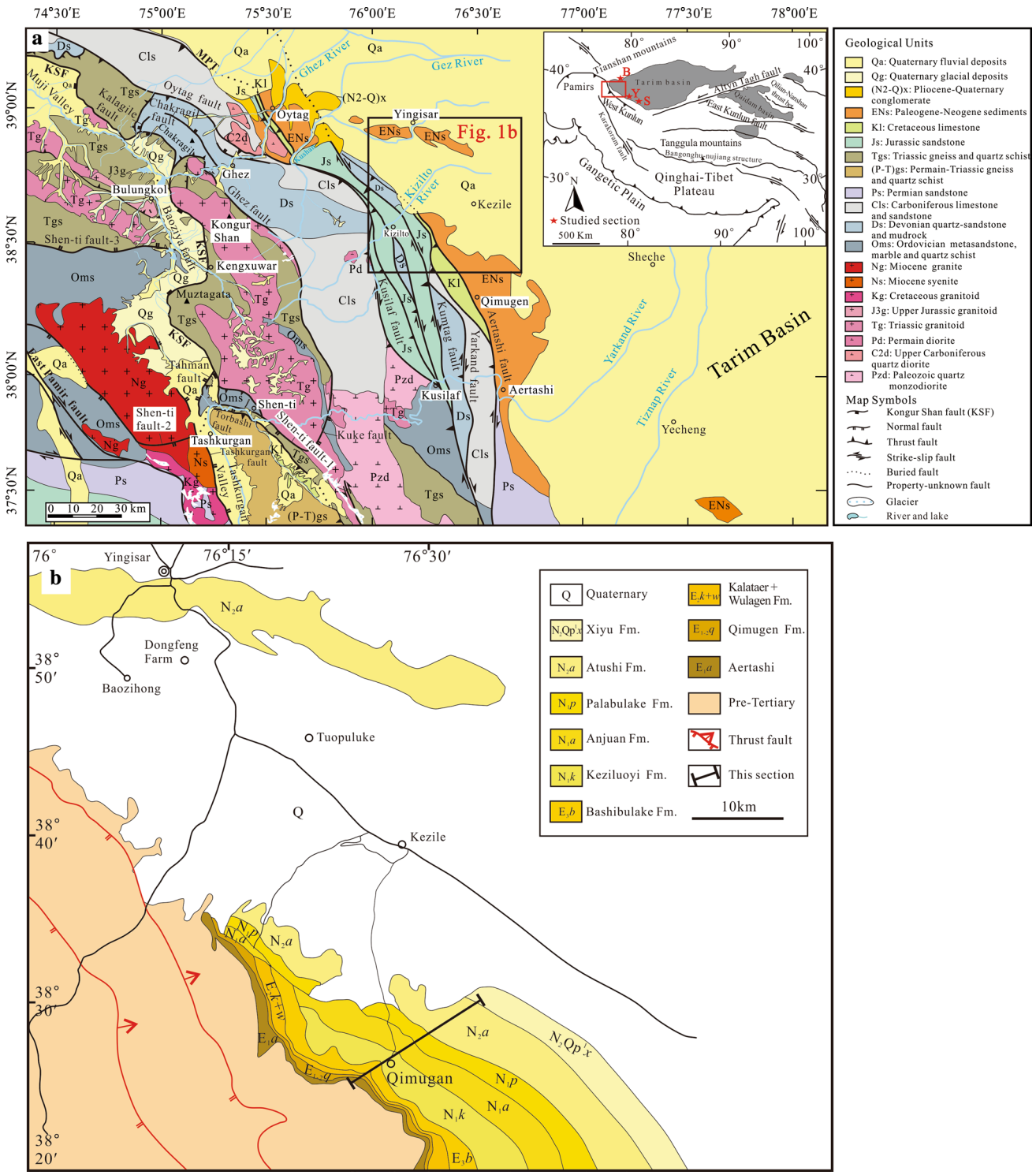

Fig. 1 **a** Schematic structural map of the Tarim Basin (Cao et al. 2013a, b); B-Boguzihe section, Y-Yecheng section, S-Sanju section; **b** detail of the location of the Qimugan section (redrawn from Wang et al. 2013a). **b** The whole section from Paleogene to Neogene, while in this study we focus on the Neogene sediments

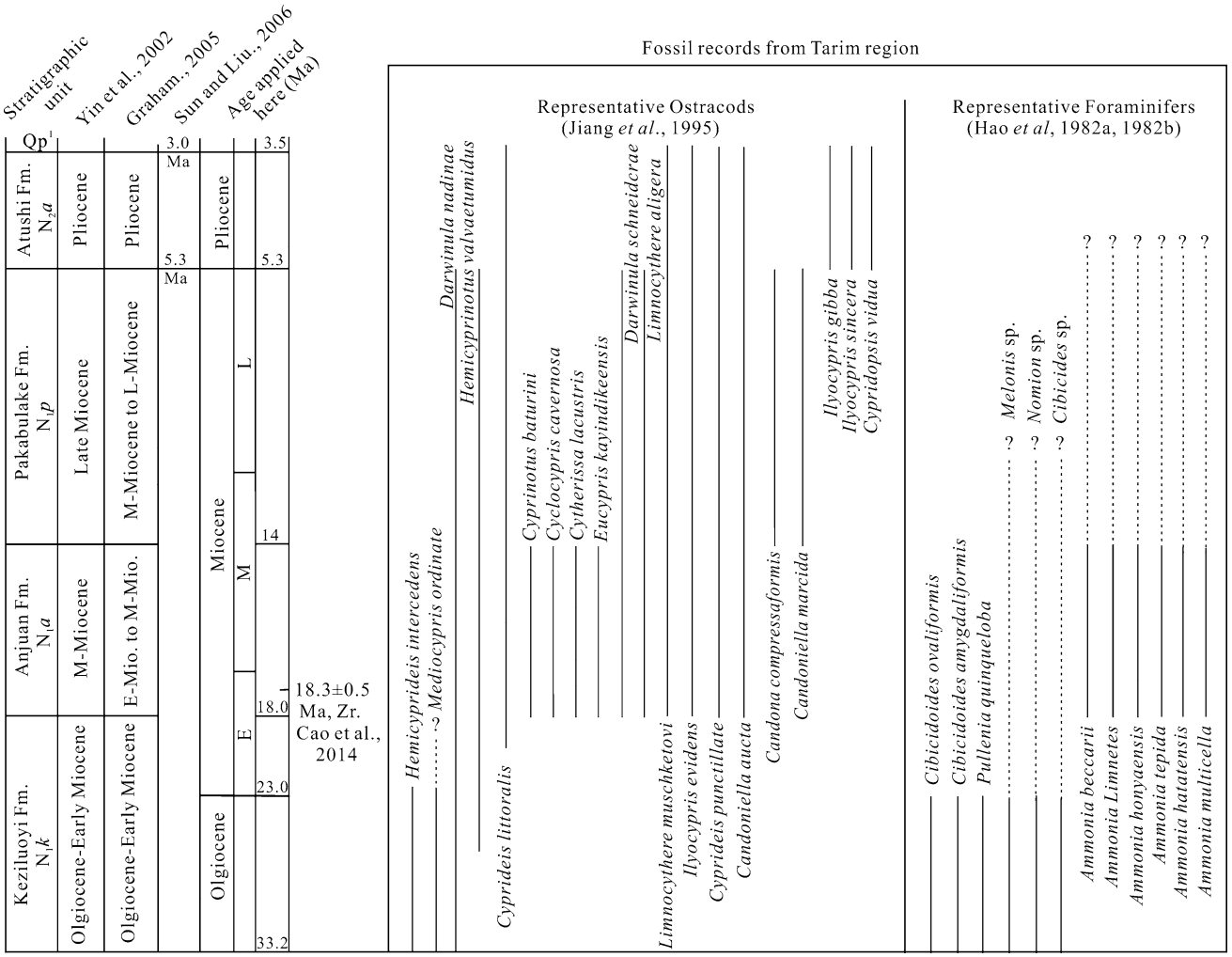

Fig. 2 Lithostratigraphic units, biostratigraphies, and chronology of Qimugan section. The Epoch and age were estimated from ostracod biostratigraphies (Jiang et al. 1995) in concert with foraminiferal biostratigraphies (Hao et al. 1982a, b) with well-dated magnetostratigraphic ages (Huang et al. 2006; Ji et al. 2008) in the Kuche Basin, the *Southwestern depression* in the Tarim Basin, and in the Qaidam and Xunhua basins (see text for detail). The symbol '?' in the figure stands for unknown presence of the fossil species. The ages applied here are in accordance with the International Chronostratigraphic Chart (ICS 2015)

Age control

The Keziluoyi, Anjuan, and Pakabulake Formations in the Qimugan section are assigned to be Oligocene to lower Miocene, middle Miocene, and upper Miocene, respectively (Fig. 2; Wang et al. 1990; Graham et al. 2005; Yin et al. 2002). These ages are based on fossils, including ostracods and benthic foraminifers. Additional magnetostratigraphic dating in the southwestern depression of Tarim Basin confirms the chronostratigraphic division of these formations. By integrating the fossil assemblages, magnetostratigraphic dating, and detrital igneous zircon chronology (Cao et al. 2014), the age uncertainty at the boundaries of each two formations should be within 1 Myr. The age uncertainties of events are within 0.5 to 1 Myr at different stratigraphic levels based on calculated results assuming the accumulation rate within each formation is invariable.

Keziluoyi and Anjuan formations

The bottom of the Keziluoyi Formation is on a regional scale characterized by an unconformity with the underlying Keziluoyi Formation (Sun and Jiang 2013; Bosboom et al. 2013). This unconformity is magnetostratigraphically dated in the Oytag and the Aertashi sections at around the boundary between the Eocene and Oligocene with the onset of sedimentation estimated consistently at ~33.2 Ma (Fig. 1a; Sun and Jiang 2013; Bosboom et al. 2013).

The dominant species of the ostracods and foraminifers in Xinjiang province, China, provide an opportunity to correlate the biostratigraphic units among the Tarim Basin,

Junggar Basin, and Kuche Depression (Jiang et al. 1995; Hao et al. 1982a, b). The Keziluoyi and Anjuan Formations can be correlated with the Shawan and Taxihe Formations in the Junggar Basin and to the Jidike Formation in the Kuche Depression. The dominant ostracod species in the lower part of the Keziluoyi Formation are *Hemicyprideis intercedens, Hemicyprinotus valvaetumidus*, *Mediocypris ordinate*, and *Darwinula nadinae*, accompanied by *Cyprideis littoralis* at the top of the Keziluoyi Formation (Fig. 2; Jiang et al. 1995). The species that only appear in the Anjuan Formation are *Cyprinotus baturini, Cyclocypris cavernosa, Cypridopsis nitida, Cytherissa lacustris, Eucypris concinna, Eucypris kayindikeensis, Leptocythere longiformis, Limnocythere dura* (Fig. 2; Jiang et al. 1995). The species above, both in the Keziluoyi and Anjuan Formations, appear in the Shawan and Taxihe Formations in the Junggar Basin, as well as in the Jidike Formation in the Kuche Basin, respectively (Fig. 2; Jiang et al. 1995). These species simultaneously disappear in the Dushanzi and Kangcun Formations, which overlie the Taxihe and Jidike Formations, respectively. Therefore, the top of the Anjuan Formation can be assigned to be late middle Miocene (~14 ± 0.5 Ma), as the boundaries between the Dushanzi and Taxihe Formations and the Kangcun and Jidike Formations were magnetostratigraphically dated as 14.5–13.5 Ma (Huang et al. 2006; Ji et al. 2008).

The lower and middle portions of Keziluoyi Formation can be assigned to be Oligocene to early Miocene in age. The specie *Hemicyprideis intercedens* appeared in the lower portions of the Keziluoyi Formation and can be found only in the Shawan and Jidike Formations, respectively. This could assign the lower portions of the Keziluoyi Formation to be as young as 22.5 Ma, which is the magnetostratigraphically dated youngest age of the Shawan Formation (Huang et al. 2006). The dominant species of the ostracods *Hemicyprinotus valvaetumidus, Hemicyprinotus sp.* as well as *Mediocypris sp.* in the middle portions of the Keziluoyi Formation were reported in the upper Shangyoushashan and Xiaganchaigou Formations in the Qaidam Basin, with an age spanning from late Oligocene to Miocene (Sun et al. 1999, 2005b). These species were also recorded in Jingou River section in Xinjiang province, with a late Oligocene age based on magnetostratigraphic dating (Dong et al. 2013). The benthic foraminifera in the lower part of the Keziluoyi Formation are abundant in *Cibicidoides ovaliformis*, *C. amygdaliformis*, *Pullenia quinqueloba*, *Melonis sp.*, *Nonion sp.*, *Cibicides sp.* (Hao et al. 1982a, b). These benthic foraminifers, especially the Cibicidoides and Cibicides fauna, are widely recorded in the Oligocene strata in American basins (Armentrout and Berta 1977).

The upper portions of the Keziluoyi Formation could have been deposited during the late early Miocene. Firstly, the specie *Mediocypris ordinate* can be found in the Taxihe and Jidike Formations, which are dated to be early to middle Miocene in age (Huang et al. 2006). Secondly, the specie *Hemicyprideis intercedens* was reported during the late Chattian (~28–23 Ma) to Aquitanian (~23–20 Ma) in central European basins based on detailed biostratigraphic correlations (Gebhardt 2003). The upper Keziluoyi Formation should thus be younger than ~20 Ma considering that the species *Mediocypris ordinate* and *Hemicyprideis intercedens* are found in its lower portions.

The benthic foraminiferal assemblage in the Anjuan Formation can further constrain the age of the upper part of the Keziluoyi Formation. The overlying Anjuan Formation dominantly contains *Ammonia beccarii* (Linné), *A. Limnetes* (Todd et Bronnimann), *A. honyaensis* (Asano), *A. tepida* (Cushman), *A. hatatensis* (Takayangi), and *A. multicella* (S. Y. Zheng) (Hao et al. 1982a, b). The most abundant species, *Ammonia beccarii*, reported in the east of the Tarim Basin, points to a middle Miocene age (Ritts et al. 2008). In the Central Paratethys, *Ammonia beccarii* is also reported at the bottom and middle parts of the combined Tengelic-2 and Tekeres-1 sections, which span from 16.4 to 13.0 Ma during the late to middle Miocene (Báldi 2006). This indicates the upper part of the Keziluoyi Formation could have been deposited between ~20–16 Ma and the top of the Anjuan Formation roughly at 14 ± 0.5 Ma, which is in line with the result of correlated ostracods among the Tarim Basin, Junggar Basin, and Kuche Depression (Jiang et al. 1995). A minimal U/Pb age of 18.3 ± 0.5 Ma for detrital zircon chronology from a sandstone bed at the base of the Anjuan Formation (Cao et al. 2014) could point to a 17 ± 1 Ma age for the sampled layer considering that the time needed for zircon exhumation and transportation (Malusà et al. 2009). With this respect, the boundary of the Keziluoyi and Anjuan Formations in the Qimugan section could be assigned to be 18 ± 1 Ma based on the accumulation rate in the Anjuan Formation, which is in line with the biostratigraphic estimates. Therefore, the Keziluoyi and Anjuan Formations can be placed in the Oligocene (33.2 Ma) to early middle Miocene (18 ± 1 Ma) and early middle Miocene (18 ± 1 Ma) to late middle Miocene (14 ± 0.5 Ma), respectively.

Pakabulake Formation

The ostracods in the Pakabulake Formation can be correlated with those in the Dushanzi and Kangcun formations in the Junggar Basin and Kuche Depression, respectively. Besides the occurrence of the genus *Ilyocypris*, species such as *Candona compressaformis*, *Candoniella marcida* that in Tarim Basin only occurred in the Pakabulake Formation can also be found in the Dushanzi and Kangcun Formations (Jiang et al. 1995), which are dated as 14.5–6.5

and 13.5–6.0 Ma, respectively (Huang et al. 2006; Ji et al. 2008). The ostracod assemblage *Ilyocypris-Cyprideis-Candona-Candoniella* in the Pakabulake Formation can also been found in the Shangyoushashan and Shizigou Formations in the Qaidam Basin and the Dongxiang, Liushucun, and Hewangjia Formations in the Xunhua Basin (Luo et al. 2010). These formations in the Qaidam and Xunhua basins are dated younger than 14–15 Ma (Fang et al. 2007; Lu and Xiong 2009) and ~14.5 Ma (Ji et al. 2010) based on magnetostratigraphy. The top of the Pakabulake Formation occurs at ~5.3 Ma (Sun and Liu 2006). Therefore, the Pakabulake Formation is interpreted to be in late middle Miocene (~14 ± 0.5 Ma) to late Miocene (~5.3 Ma).

Atushi Formation

The age of the Atushi Formation varies depending on geographic location. In the Tarim Basin (Fig. 1), magnetostratigraphic studies have demonstrated that the Atushi Formation is >4.6–3.5 Ma in the Yecheng section (Zheng et al. 2000, 2010), ~5.3–3.0 Ma in the Sanju section (Sun and Liu 2006; Sun et al. 2008), and >5.5–2 Ma in the western Boguzihe section (Zhang et al. 2013). However, there is an angular unconformity between the Pakabulake and the overlying Atushi Formations in the Sanju section (Sun et al. 2008), while it is a conformable contact in the Yecheng and studied sections (Zheng et al. 2000, 2010). We therefore use the age model of the Yecheng section to constrain the minimum age, and the Sanju section to constrain the maximum age of the base of the Atushi Formation, because these two sections are within 200 km to the Qimugan section used in this study (Fig. 1). The ostracod assemblage broadly supports this age model. The identified species in Atushi Formation are *Ilyocypris gibba*, *I. sincera*, *Crypridopsis regularis*, *C. vidua*, *Candoniella aucta*, *C. kasachstanica*, *Eucypris notabilis*, and *Condona grum-grijimailoi* (Jiang et al. 1995). The species *Ilyocypris gibba* was recorded in the Baccinello–Cinigiano Basin (Tuscany, central Italy) since the early Messinian (Ligios et al. 2008). Some of these fossils, such as *Cypridopsis vidua* and *Ilyocypris sincera* (Jiang et al. 1995), are abundant in the Kuche Depression with an age of <~6 Ma (Zhang et al. 2013; Huang et al. 2006). The Atushi Formation is likely latest Miocene or early Pliocene (~5.3 Ma) to middle Pliocene (3.5 Ma).

Materials and methods

Sampling and section

The Materials and methods of previous whole-rock mineralogical, clay mineralogical, and geochemical data are given in Wang et al. (2013a) and Cao et al. (2014). For parts of the minor elemental data, the same samples of the Qimugan section in the Tarim Basin were analyzed, and the reported stratigraphic levels follow those of Wang et al. (2013a). The base of the discussed part of the section therefore occurs at stratigraphic level 1205.1 m and the top at 2959.9 m. All 73 samples are composed of fine-grained sediments, including 64 mudstones and 9 siltstones.

Minor elements and chemical weathering indices

The detailed descriptions of sample preparation and measurement are given in Cao et al. (2014). Fine-grained rocks (mudstone) were selected without sand fractions to limit the influence of sediment sorting and diagenesis (Blatt and Sutherland 1969; Zhang et al. 2002). The Ba, Ni, Cr, and Co are listed in Table 1.

Using published (Cao et al. 2014) and new data, elemental ratios Na/Al, Na/Ti, and Ba/Sr were calculated (Table 1). Besides the chemical weathering indices CIA, CIW, and CIW′ provided by Cao et al. (2014), we also evaluated the effect of diagenesis by calculating the plagioclase index of alteration (PIA: formula 1, Table 1), as potassium is enriched in sediments during diagenesis (Fedo et al. 1995; Harnois 1988).

$$\mathrm{PIA} = 100 \times \{(\mathrm{Al_2O_3} - \mathrm{K_2O})/[(\mathrm{Al_2O_3} - \mathrm{K_2O}) + \mathrm{CaO} * + \mathrm{Na_2O}]\} \quad (1)$$

The elemental abundances are expressed as molar proportions when calculating CIA, PIA, CIW, and CIW′, and CaO* represents the Ca associated with silicate minerals without carbonate and apatite fractions of the sediment (Nesbitt and Young 1982). Following McLennan (1993), we use the molar proportion of Na_2O instead of the molar proportion of CaO from the silicate fraction, because both calcite and dolomite are present in the samples. This method results in less certain absolute estimates of chemical weathering, while the trends along the section can still be evaluated.

Mineral morphology

Scanning electron microscopy was used to study the morphology of clay minerals, in order to further trace the mineralogical change associated with changes in weathering. Few grams of sediment was platinum-coated for SEM observation of mineral morphology. The analyses were carried out at Materials Science and Engineering Test Center, Wuhan University of Technology, Wuhan, China, using a JSM-5610 scanning electron microscope at 20 kV accelerating voltage and a beam current in the range of 1–3 nA.

Table 1 Analyzed and calculated chemical data of sediments at different stratigraphic levels

Sample	Thickness	Na/Ti	Na/Al	Ba	Ba/Sr	PIA	Cr	Co	Ni	Cr/UCC	Co/UCC	Ni/UCC
S3HM-58-1	1205.1	3.73	0.23	335.0	3.64	61.95	64.3	15.8	42.2	0.77	0.93	0.96
S3HM-59-1	1218.8	3.97	0.24	402.0	3.44	60.67	89.6	19.0	50.1	1.08	1.12	1.14
S3HM-60-1	1245.0	2.65	0.15	438.0	3.84	71.09	91.9	22.0	52.9	1.11	1.29	1.20
S3HM-61-1	1293.9	2.77	0.16	397.0	3.89	69.69	79.9	19.3	49.3	0.96	1.14	1.12
S3HM-62-1	1309.1	2.75	0.17	393.0	3.78	69.06	68.4	17.5	45.8	0.82	1.03	1.04
S3HM-62-1	1310.7	3.36	0.21	358.0	3.28	63.90	69.3	16.9	43.3	0.83	0.99	0.98
S3HM-63-1	1327.1	2.78	0.15	460.0	4.11	71.28	84.2	19.8	50.9	1.01	1.16	1.16
S3HM-63-2	1332.5	4.99	0.32	314.0	2.80	54.79	57.2	12.3	30.8	0.69	0.72	0.70
S3HM-64-1	1354.7	4.65	0.30	361.0	2.89	56.58	55.1	12.5	31.0	0.66	0.74	0.70
S3HM-66-1	1432.1	3.36	0.19	439.0	2.76	66.03	86.2	18.8	48.4	1.04	1.11	1.10
S3HM-67-1	1439.3	3.22	0.17	510.0	4.51	68.43	95.4	24.0	58.0	1.15	1.41	1.32
S3HM-68-1	1466.6	2.77	0.16	449.0	3.10	69.72	81.3	18.6	45.4	0.98	1.09	1.03
S3HM-69-1	1467.6	3.82	0.22	422.0	3.46	62.32	67.4	15.1	39.0	0.81	0.89	0.89
S3HM-70-1	1479.9	2.46	0.13	451.0	3.24	73.99	81.7	19.6	47.5	0.98	1.15	1.08
S3HM-71-1	1489.1	8.42	0.49	428.0	3.45	43.00	70.4	19.8	55.3	0.85	1.16	1.26
S3HM-72-1	1509.0	4.37	0.25	423.0	2.82	59.52	69.4	15.2	37.5	0.84	0.89	0.85
S3HM-73-1	1553.9	4.28	0.22	418.0	2.56	61.81	56.2	12.8	33.8	0.68	0.75	0.77
S3HM-74-1	1565.7	4.92	0.34	1063.0	3.17	54.19	37.9	8.9	23.8	0.46	0.52	0.54
S3HM-75-1	1579.4	4.69	0.30	443.0	2.65	55.83	55.5	11.5	28.9	0.67	0.68	0.66
S3HM-76-1	1590.5	3.66	0.22	397.0	1.43	63.52	56.7	13.2	32.3	0.68	0.78	0.73
S3HM-77-1	1610.9	4.91	0.34	1133.0	4.43	54.05	49.4	10.6	26.9	0.60	0.62	0.61
S3HM-78-1	1629.7	4.25	0.27	495.0	2.14	58.52	56.5	12.3	31.8	0.68	0.72	0.72
S3HM-78-2	1630.5	4.08	0.27	375.0	1.09	58.84	50.0	11.1	27.8	0.60	0.65	0.63
S3HM-80-1	1669.2	3.38	0.19	623.0	0.35	65.87	60.9	14.7	35.3	0.73	0.86	0.80
S3HM-81-1	1673.8	3.95	0.23	424.0	1.53	62.42	72.9	17.0	41.7	0.88	1.00	0.95
S3HM-82-1	1717.0	5.21	0.35	468.0	1.71	53.23	54.6	10.6	29.8	0.66	0.62	0.68
S3HM-83-1	1722.9	4.02	0.22	391.0	1.25	63.09	91.5	19.4	48.5	1.10	1.14	1.10
S3HM-84-1	1801.1	5.93	0.38	402.0	0.52	50.39	46.9	9.4	23.3	0.57	0.55	0.53
S3HM-85-1	1816.6	6.78	0.42	178.0	0.10	48.41	22.1	5.6	14.1	0.27	0.33	0.32
S3HM-86-1	1822.4	4.28	0.30	301.0	0.13	55.22	32.5	7.6	22.0	0.39	0.44	0.50
S3HM-87-1	1856.9	7.01	0.45	397.0	1.53	47.91	62.9	14.9	34.3	0.76	0.88	0.78
S3HM-88-1	1868.45	14.21	1.07	396.0	0.22	27.41	35.6	7.5	20.4	0.43	0.44	0.46
S3HM-89-1	1888.9	3.70	0.21	545.0	1.36	64.47	78.8	18.2	42.3	0.95	1.07	0.96
S3HM-90-1	1900.6	5.13	0.37	438.0	1.19	52.09	53.4	9.7	28.6	0.64	0.57	0.65
S3HM-91-1	1954.9	3.18	0.17	418.0	2.30	68.42	95.3	24.6	61.0	1.15	1.45	1.39
S3HM-92-1	1998.0	4.63	0.37	934.0	0.63	51.92	41.4	8.4	22.0	0.50	0.49	0.50
S3HM-93-1	2056.6	4.53	0.30	426.0	0.48	56.37	62.0	13.7	33.3	0.75	0.81	0.76
S3HM-94-1	2067.1	3.33	0.19	443.0	3.38	66.66	94.0	20.7	50.6	1.13	1.22	1.15
S3HM-95-1	2121.8	5.25	0.32	456.0	2.90	56.20	74.0	17.5	39.4	0.89	1.03	0.90
S3HM-96-1	2155.4	3.66	0.21	432.0	2.15	64.18	81.9	18.9	44.4	0.99	1.11	1.01
S3HM-96-2	2157.6	4.47	0.28	950.0	3.63	56.67	71.5	13.5	35.7	0.86	0.79	0.81
S3HM-97-1	2195.6	3.90	0.25	318.0	0.45	61.57	50.4	12.1	29.2	0.61	0.71	0.66
S3HM-98-1	2222.5	6.13	0.35	588.0	0.23	51.78	31.5	7.2	18.1	0.38	0.42	0.41
S3HM-99-1	2231.5	21.35	1.47	480.0	0.20	20.71	30.3	7.5	19.0	0.37	0.44	0.43
S3HM-100-1	2282.3	4.05	0.30	322.0	0.55	56.16	42.0	8.8	22.8	0.51	0.52	0.52
S3HM-101-1	2332.6	3.54	0.21	461.0	2.85	63.69	90.4	18.5	47.5	1.09	1.09	1.08
S3HM-102-1	2345.8	5.93	0.39	260.0	0.29	49.45	28.4	6.2	15.5	0.34	0.36	0.35
S3HM-104-1	2393.6	3.94	0.23	336.0	1.01	61.99	67.9	16.4	35.5	0.82	0.96	0.81

Table 1 continued

Sample	Thickness	Na/Ti	Na/Al	Ba	Ba/Sr	PIA	Cr	Co	Ni	Cr/UCC	Co/UCC	Ni/UCC
S3HM-105-1	2423.0	3.73	0.21	474.0	2.82	63.64	89.4	23.0	47.0	1.08	1.35	1.07
S3HM-106-1	2456.6	5.74	0.36	342.0	0.59	54.69	47.1	11.0	29.9	0.57	0.65	0.68
S3HM-107-1	2478.7	3.74	0.20	496.0	3.82	65.13	103.2	21.8	55.3	1.24	1.28	1.26
S3HM-108-1	2498.4	3.85	0.21	467.0	3.13	63.60	94.5	14.5	41.0	1.14	0.85	0.93
S3HM-109-1	2529.4	4.74	0.29	301.0	0.40	58.13	49.5	11.5	30.0	0.60	0.68	0.68
S3HM-110-1	2570.9	5.24	0.32	428.0	1.51	54.96	70.5	17.5	40.2	0.85	1.03	0.91
S3HM-111-1	2595.5	4.70	0.30	376.0	0.59	53.96	41.9	11.0	27.3	0.50	0.65	0.62
S3HM-111-2	2596.2	4.70	0.27	301.0	0.73	59.30	65.2	14.3	39.7	0.79	0.84	0.90
S3HM-112-1	2603.0	3.41	0.21	301.0	0.65	64.04	50.5	12.2	30.3	0.61	0.72	0.69
S3HM-113-1	2631.9	4.76	0.29	654.0	2.51	56.96	61.6	12.3	33.6	0.74	0.72	0.76
S3HM-114-1	2647.8	3.60	0.21	340.0	0.78	63.97	50.6	11.5	29.4	0.61	0.68	0.67
S3HM-115-1	2657.8	5.45	0.35	570.0	1.25	52.78	51.5	10.9	28.1	0.62	0.64	0.64
S3HM-115-2	2659.9	4.93	0.30	460.0	0.92	56.47	68.6	14.4	36.6	0.83	0.85	0.83
S3HM-116-1	2665.8	3.03	0.16	393.0	1.16	70.36	63.2	15.1	36.2	0.76	0.89	0.82
S3HM-117-1	2674.3	3.50	0.20	468.0	1.25	67.36	63.8	12.4	34.5	0.77	0.73	0.78
S3HM-117-2	2687.6	3.83	0.25	367.0	0.77	62.14	40.7	16.7	28.4	0.49	0.98	0.65
S3HM-118-1	2698.2	3.22	0.17	393.0	1.41	70.05	78.4	19.2	38.2	0.94	1.13	0.87
S3HM-119-1	2724.3	3.93	0.23	455.0	2.07	64.07	66.3	17.2	33.3	0.80	1.01	0.76
S3HM-120-1	2769.9	2.74	0.16	514.0	2.40	70.14	71.7	16.9	35.9	0.86	0.99	0.82
S3HM-121-1	2794.4	3.57	0.19	572.0	2.76	66.81	80.9	20.0	43.4	0.97	1.18	0.99
S3HM-122-1	2849.5	3.26	0.20	394.0	2.08	66.17	70.6	16.2	37.3	0.85	0.95	0.85
S3HM-123-1	2879.9	3.01	0.19	329.0	1.52	67.16	92.3	19.5	52.2	1.11	1.15	1.19
S3HM-124-1	2883.6	4.18	0.26	388.0	1.72	61.17	58.4	15.4	29.1	0.70	0.91	0.66
S3HM-125-1	2921.2	3.46	0.22	366.0	2.00	63.67	69.7	16.4	39.0	0.84	0.96	0.89
S3HM-126-1	2959.9	6.42	0.43	747.0	2.67	48.69	47.5	12.0	26.2	0.57	0.71	0.60
Min.		2.46	0.13	178.0	0.10	20.71	22.1	5.6	14.1	0.27	0.33	0.32
Max.		21.35	1.47	1133.0	4.51	73.99	103.2	24.6	61.0	1.24	1.45	1.39
Average		4.59	0.29	454.6	1.99	59.60	64.3	14.8	36.3	0.77	0.87	0.82

The other elemental ratios, chemical weathering indices, and mineralogical data plotted in Figs. 3 and 4 refer to Cao et al. (2014) and Wang et al. (2013a, b), respectively, and are not listed here. Note that the concentrations of Ni, Co, Cr in Upper Crust Composition (UCC) are from McLennan (2001). The data from samples S3HM-71-1 and S3HM-99-1 are not plotted in Figs. 3 and 4 as these results are biased due to high proportions of halite (Wang et al. 2013a)

Statistics

In order to discuss long-term trends, nine-point moving averages and their standard deviation windows were calculated after re-sampling the data series with equal intervals using the program AnalySeries 1.1.1 (Paillard et al. 1996), in which a linear function was adopted. To convey the robustness of the trends, standard deviation windows of each nine-point data were calculated by Microsoft Office Excel 2010.

Results

Geochemical results

The ratios of Ba/Sr, Rb/Sr, Cr/UCC, Co/UCC, and Ni/UCC exhibit decreasing trends from 33.2 to 14.5 ± 0.5 Ma followed by an interval with low values between 14.5 ± 0.5 and 13 ± 0.5 Ma (Figs. 3, 4). The CIA, PIA, CIW, and CIW′ indices show similar decreasing trends from 33.2 Ma onwards with minimal values reached between 14 ± 0.5 and 13 ± 0.5 Ma with that showing a small delay compared to the previously mentioned chemical ratios. The trace elements Co, Cr, and Ni are close to UCC values between 33.2 and 17 ± 1 Ma and lower than UCC afterward. The CIA values range from 48 to 66 between 33.2 and 13 ± 0.5 Ma, which represent low-to-moderate degrees of chemical weathering (Fedo et al. 1995). In contrast, the ratios of Na/Al and Na/Ti display increasing trends from 33.2 to 14 ± 0.5 Ma. Similar, but opposite to the CIA, PIA, CIW, CIW′ indices, maximal values in Na/Al and Na/Ti are reached between 14 ± 0.5 and 13 ± 0.5 Ma.

Superimposed on these general trends, a pronounced shift occurs at ~17 ± 1 Ma among above indices. Mean

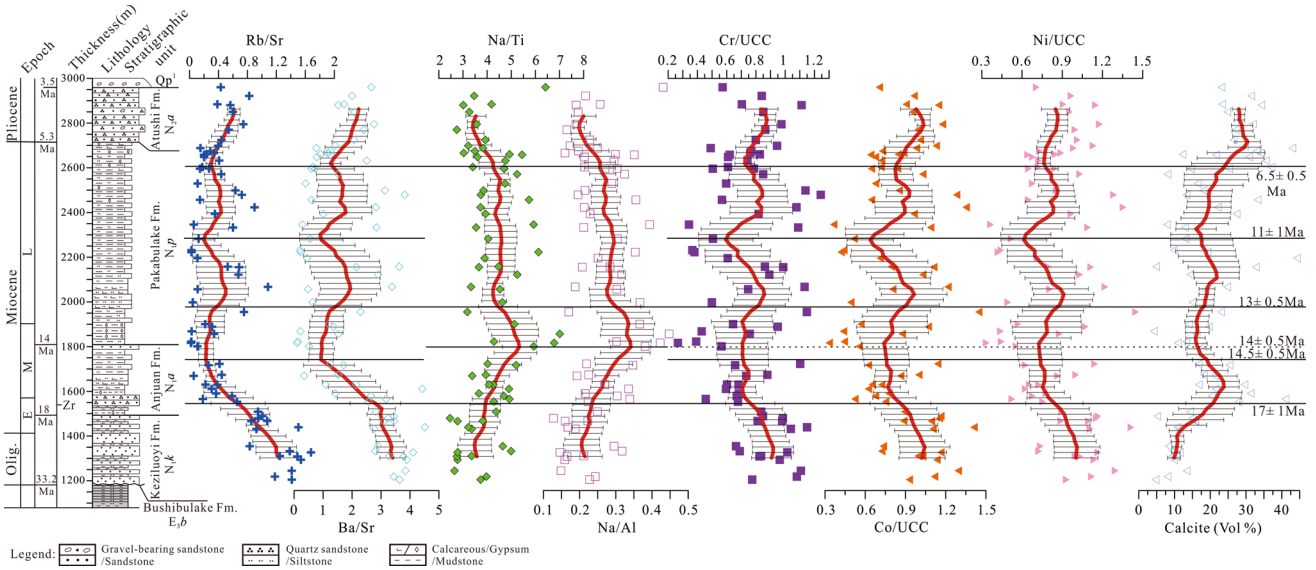

Fig. 3 Elemental ratios plotted against stratigraphic position in the Qimugan section, Tarim Basin, China. The *red line* gives nine-point moving average of the re-sampled data calculated from the program AnalySeries 1.1.1. The uncertainty bars are the standard deviation of each adjacent nine points of the re-sampled data. The calcite contents from the same section are also included for comparison (Wang et al. 2013a). Note that remarkable shifts are observed among all the indices at 17 ± 1 and 6.5 ± 0.5 Ma, respectively. Increased Na/Ti, and Na/Al, and decreased Rb/Sr and Ba/Sr, as well as Co/UCC, Cr/UCC, and Ni/UCC occur at 17 ± 1 Ma, while these indices reverse at 6.5 ± 0.5 Ma, except that the calcite increases again

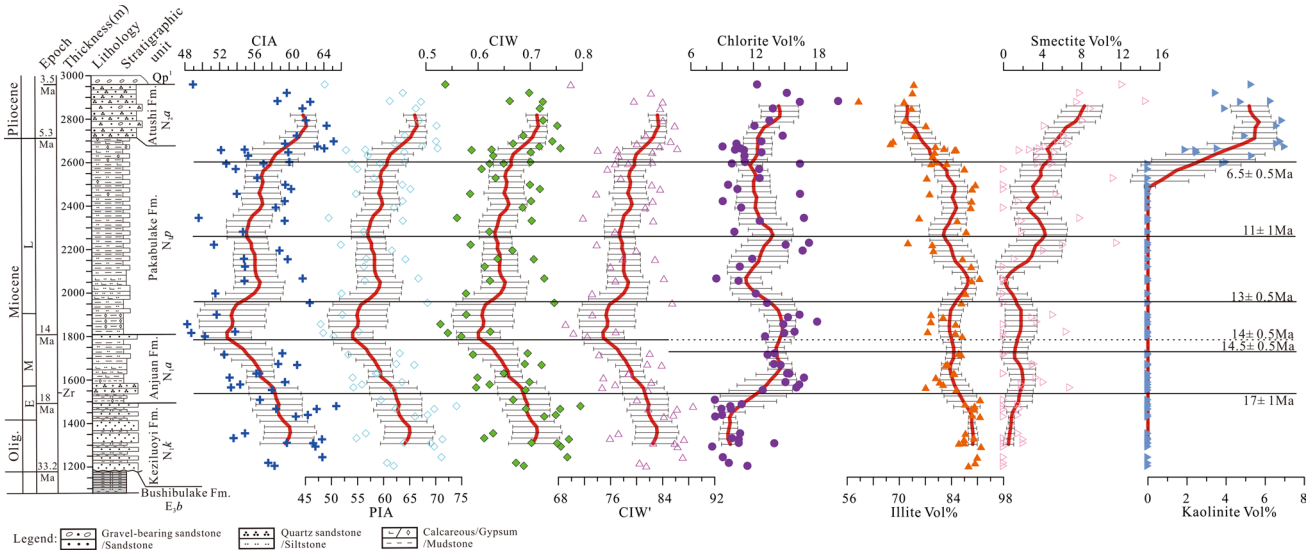

Fig. 4 Chemical weathering indices CIA, PIA, CIW and CIW′ and the relative proportions of clay minerals plotted against stratigraphic position in the Qimugan section, Tarim Basin. The red line gives nine point moving average of the re-sampled data calculated from the program AnalySeries 1.1.1. The uncertainty bars are the standard deviation of each adjacent nine points of the re-sampled data. Clay mineralogy data are from Wang et al. (2013a). *Note* the distinct decreases in chemical weathering indices and increases in chlorite and smectite are observed at 17 ± 1 Ma. The chemical weathering indices, chlorite, smectite, and kaolinite contents increase at 6.5 ± 0.5 Ma, while the illite content decreases

values before and after 17 Ma show dramatic decreases in the Ba/Sr and Rb/Sr ratios by 0.8 (66 %) and 1.3 (40 %), and the Cr/UCC, Co/UCC, and Ni/UCC ratios by 33, 29, and 33 %. The Na/Al and Na/Ti ratios show gently decreasing patterns across the distinct shifts of the CIA, PIA, CIW, and CIW′ indices at 17 Ma.

Na/Ti and Na/Al ratios, and CIA, PIA, CIW, and CIW′ indices exhibit inverse trends between 13 ± 0.5 and

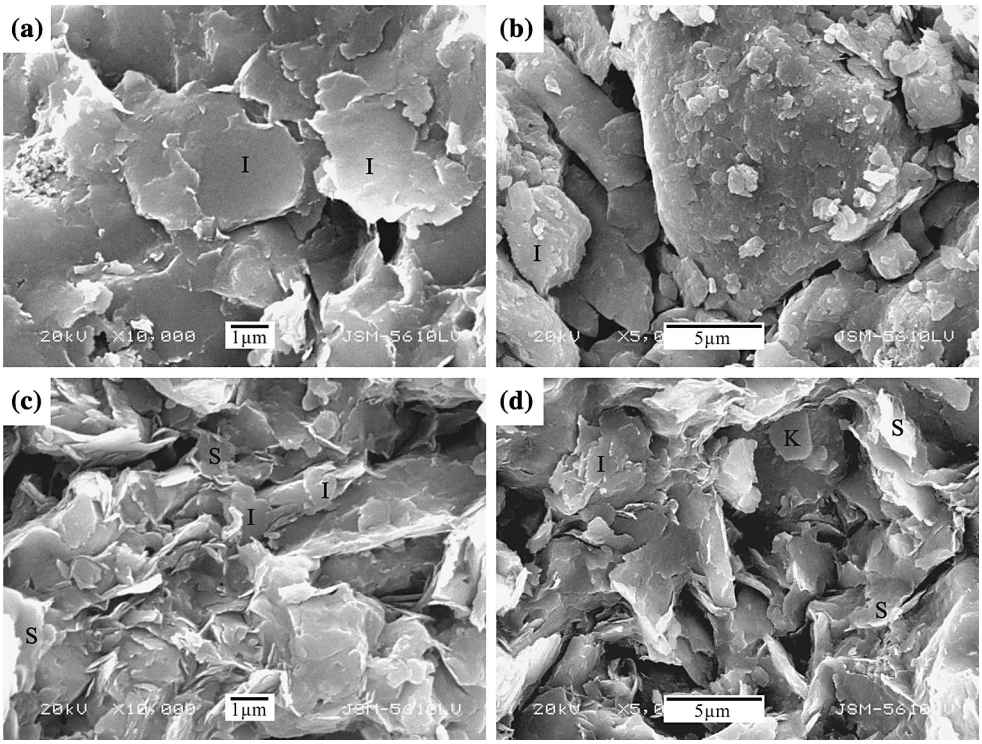

Fig. 5 Scanning electron photographs at different stratigraphic levels. **a** Sample No. S3-67-1 location 1439.3 m; **b** Sample No. S3-86-1 location 1822.4 m; **c** Sample No. S3-106-1 location 2456.6 m; **d** Sample No. S3-120-1 location 2769.9 m. Note that the clay morphology changes from poorly developed lateral thickness, thin plates, and embayed edges before 17 ± 1 Ma (**a**) to thicker plates and rounded outlines (**b**) after 17 ± 1 Ma. The clay minerals display rounded aggregates before 6.5 ± 0.5 Ma (**c**) and thin plates and embayed edges after 6.5 ± 0.5 Ma (**d**). *I* stands for illite, *S* for smectite, and *K* for Kaolinite

3.5 ± 0.5 Ma compared to the older interval (Figs. 3, 4) with the ratios decreasing and the indices increasing. Rb/Sr, Ba/Sr, Cr/UCC, Co/UCC, and Ni/UCC ratios are relatively stable between 13 and 6.5 Ma and slightly increase afterward. At 11 Ma, a single low interval occurs in Rb/Sr, Ba/Sr, Cr/UCC, Co/UCC, and Ni/UCC ratios. The trace elemental, Co, Cr, Ni, abundance remains below the UCC (McLennan 2001) in this interval until 6.5 Ma and slightly increase afterward. The CIA values range from 49 to 65 between 13 ± 0.5 and 3.5 ± 0.5 Ma, representing low-to-moderate degrees of chemical weathering.

A significant shift starts at 6.5 ± 0.5 Ma in the topmost part of the Pakabulake Formation and ends in the Atushi Formation in all measured proxy indices. Coincident small increases occur in the Rb/Sr, Ba/Sr, Cr/UCC, Co/UCC, and Ni/UCC ratios. More pronounced at 6.5 Ma are the 22 % and 25 % respective decreases in the Na/Al and Na/Ti ratios and the 5–8 % increases in the CIA, PIA, CIW, and CIW′ weathering indices.

Mineralogical results

The illite content exhibits a decreasing trend from 33.2 to 17 ± 1 Ma followed by an interval with low values between 17 ± 1 and 13 ± 0.5 Ma (Figs. 3, 4). In contrast, the contents of calcite, chlorite, and smectite display increasing trends from 33.2 to 17 ± 1 Ma. The chlorite and smectite contents reach a period of maximal values between 17 ± 1 and 13 ± 0.5 Ma, while the calcite contents increase between 17 ± 1 and 14.5 ± 0.5 Ma and decrease between 14.5 ± 0 and 13 ± 0.5 Ma.

Similar to the geochemical indices, a pronounced shift occurs at ~17 ± 1 Ma among above mineralogical indices. Mean values before and after 17 Ma show a decrease in illite content by 6 % and increases in calcite and chlorite contents by 10 and 5 %, respectively, compared to their initial values. A negligible increase in smectite occurs. The illite content shows a decreasing trend since 13 ± 0.5 Ma, while the smectite and calcite contents show a reverse trend. Chlorite and kaolinite are relatively stable between 13 ± 0.5 and 6.5 ± 0.5 Ma. At 6.5 ± 0.5 Ma, calcite contents increase by 10 %, kaolinite by 5 %, smectite by 4 %, and chlorite by 2 %, while illite contents decrease by 11 %. A single low interval occurs in calcite and illite at 11 Ma, while chlorite and smectite show a short-term high at this time.

Clay minerals display different morphologies below and above the shift at 17 ± 1 Ma. Below, the clay minerals

present poorly developed lateral thickness, thin plates, and embayed edges (Fig. 5a, 1439.3 m). This indicates the clay minerals formed under relative intense chemical weathering from dissolution and hydrolysis (Hong et al. 2007; Wang et al. 2013a, b). Above, clay minerals occur as aggregates filling the interstitial space between detrital particles and show thicker plates and rounded outlines (Fig. 5b, 1822.4 m). This suggests the clays formed under much weaker chemical weathering (Wang et al. 2013a, b). Clay minerals reveal distinct morphology before and after 6.5 ± 0.5 Ma. The clay minerals display rounded aggregates before 6.5 ± 0.5 Ma (Fig. 5c, 2456.6 m), suggesting physical weathering dominating the weathering process. After 6.5 Ma, the morphology of the clays shows similar characteristic as before 17 ± 1 Ma, showing thin plates and embayed edges (Fig. 5d, 2769.9 m). This suggests enhanced chemical weathering or enhanced influx of chemical weathering products during this period.

Discussion

We discuss, first, interpretation possibilities of the geochemical and clay mineralogical proxies, and second, the 17, 11, and 6.5 Ma changes observed in the section in the western Tarim Basin, China.

Evaluation of environmental and provenance proxies

Chemical weathering indices are affected by climate, hydraulic sorting, diagenesis, and changing sediment provenance (Fralick and Kronberg 1997). In our study, sample preparation was done such that hydraulic sorting can be neglected. Diagenesis is thought to not be dominant. First, because the sediment samples exhibit unsolidified texture with poor cementing (Fig. 5). Second, because diagenesis can yield elevated potassium concentrations in paleosols, resulting in higher illite proportions and higher crystallinity with depth (Drits et al. 2002; Warr and Rice, 1994) both not seen in our samples (Fig. 4; Wang et al. 2013a). Moreover, the mature R1 illite-rich mixed layer, which is typically of diagenetic origin (Perry and Hower 1970), is not seen in the deposits. Third, because the CIA value can be affected by potassium enrichment (Fedo et al. 1995), while CIA here covaries with PIA, CIW, and CIW′ indicating potassium enrichment lacks or has been limited. And, fourth, because fossil shells of Eocene sediments in the nearby Aertashi section have shown limited calcite diagenesis (Bougeois et al. 2014).

Sediments deposited along the northwestern margin of the QTP can be useful indicators for its uplift history, especially if the products formed under weak chemical and strong physical weathering (Métivier et al. 1998; Yin et al. 2002). These products can better maintain the original elemental composition of the source rock and studies of sediment provenance can be performed. Some elements, such as K, Rb, and Ba, can become depleted after extreme chemical weathering (Condie et al. 1995). Here, the values of the CIA weathering index indicates low-to-intermediate weathering levels through the section, in line with the PIA, CIW, and CIW′ indices. This indicates that these sediments are texturally, petrographically and chemically immature and Ba/Sr and Rb/Sr ratios can likely be used as provenance proxies (Borges et al. 2008). The addition of feldspar usually rich in Ba and Rb (Zhang et al. 2002) and reworked secondary carbonate usually rich in Sr (Buggle et al. 2011) changes these ratios.

Provenance and climate change at ~17 Ma

A dramatic shift occurs in the geochemical trace element, mineralogical records, and clay morphologies of the Qimugan section at ~17 Ma ± 1 Myr in the latest early Miocene or late Burdigalian (Figs. 3, 4). We interpret this shift to be a change in provenance causing increasing amounts of sediments rich in carbonates. The simplest way to explain the observed findings is exposure and re-deposition of older Paleogene sediment in the Qimugan section in combination with additional exposure of gneisses and schists along the Pamir and West Kunlun ranges during the middle Miocene. The Paleogene marine sediments are rich in carbonate and with that Sr, and rich in smectite (Wang et al. 2013a) in line with the increases in calcite, smectite, and decreases in the Rb/Sr and Ba/Sr ratios. Also, the decreasing concentrations of immobile elements Co, Cr, and Ni relative to the Upper Crustal Composition (UCC) are in line with this interpretation as these are usually low in carbonates (Parekh et al. 1977; Woolley and Kempe 1989). The increase in chlorite, however, cannot be explained by re-deposition of the Paleogene sediments. Chlorite is a useful proxy for physical erosion in the source as it is derived from erosion of low- and medium-grade metamorphic rocks (Hurlbut and Klein 1985) and not resistant to hydrolysis (Chamley 1989). The simultaneous increases in chlorite and smectite contents seem contradictory as the low resistance to hydrolysis causes chlorite to occur in cold and dry environments, while smectite forms in temperate environments (Robert and Kennett 1997). The simultaneous increase in chlorite and smectite can thus best be explained by enhanced physical erosion of different sources. With the smectite being derived from the Paleogene sediments, the chlorite is likely derived from the Pamir and West Kunlun ranges.

The shifts in geochemical indices and mineralogical composition indicate the change of provenance is the dominant factor at the boundary 17 ± 1 Ma. Climate change could be a secondary factor affecting the data. The CIA shows low

values between 48 and 66 in all samples. The values of CIA are much lower between 17 ± 1 and 13 ± 0.5 Ma than before 17 ± 1 Ma (Fig. 4). This is against the increases in chlorite (CIA = 100) and smectite (CIA = 70–80) contents, and decreases in illite (CIA = 70–80) and feldspar (CIA = 50) contents (Wang et al. 2013a). The lower CIA values between 17 and 13 Ma can therefore not be explained by the observed provenance change. Major element analysis shows the decrease in CIA is mainly due to a decrease in Al_2O_3 content (Cao et al. 2014). Aluminum and titanium are immobile during chemical weathering processes, and will be enriched in residues compared with parent rocks and sediments (Buggle et al. 2011; Nesbitt and Markovics 1980). The decrease in CIA, PIA, CIW, and CIW′ could be best explained by a weakened chemical weathering in line with the changes in clay morphology showing occurrence as aggregates filling the interstitial space between detrital particles and having thicker plates and rounded outlines after 17 Ma (Fig. 5b). Weakened chemical weathering could also explain the decrease in TiO_2 observed after 17 ± 1 Ma (Cao et al. 2014). The decrease in Al and Ti contents results in increases in Na/Al and Na/Ti ratios between 17 ± 1 and 13 ± 0.5 Ma (Fig. 3). Besides the indices above, the increase in chlorite content also indicates a weakened chemical weathering as chlorite is mainly preserved under cool and dry climatic conditions (Vanderaveroet 2000; Winkler et al. 2002). The Ba/Sr and Rb/Sr ratios can be affected by a change in provenance, while the dramatic decrease in these ratios is likely amplified by an additional effect of climate cooling and drying after 17 ± 1 Ma, leading to less leaching of Sr (Buggle et al. 2011; Nesbitt and Markovics 1980). These observations suggest that the climate became cooler and drier after 17 ± 1 Ma, following the active tectonics in the middle Miocene (e.g., Amidon and Hynek 2010; Sobel and Dumitru 1997).

The changes of the climate-controlled proxies Na/Al and Na/Ti, and CIA, PIA, CIW, and CIW′ show different patterns compared to the proxies controlled by provenance Co/UCC, Cr/UCC, Ni/UCC, Rb/Sr, Ba/Sr, calcite, chlorite, and smectite. The climate-controlled proxies exhibit gradual trends in contrast to the more dramatic changes in the provenance-controlled indices. Moreover, the climate proxies reach peak values at 14 ± 0.5 Ma, slightly later than the provenance-controlled indices. Also, the provenance-controlled indices reach maximal or minimal transient peak values at 11 ± 1 Ma, while the climate-controlled indices show no or only slight changes at this time. These differences support climate being the most dominant factor controlling Na/Al, Na/Ti, CIA, PIA, CIW, and CIW′.

Provenance change at ~6.5 Ma

Starting at 6.5 Ma in the top of the Pakabulake Formation, another significant shift occurs in the Qimugan section in the geochemical and mineralogical records. Taking all changes in proxy records together, we again interpret this shift to be caused by a change in provenance with additional impact of climate change. Climate is reported to change to more arid conditions in the Tarim Basin after late Miocene/Pliocene time (Graham et al. 2005; Sun et al. 2008; Chang et al. 2013). The increased chemical weathering of clay minerals must therefore be explained by increased flux of chemically weathered minerals as their structure may be maintained (Fig. 5c, d). The addition of sedimentary sources must, besides being rich in chemical weathering products, be rich in Co, Cr, and Ni, and in calcite and kaolinite, of which the latter two were found in the Paleogene sediments of the Qimugan section. This new sedimentary source might be combined eolian sediments and Paleogene sediments, as, firstly, eolian input is reported to initiate in the Tarim Basin during the latest Miocene to Pliocene (Sun and Liu 2006; Sun et al. 2009) and, secondly, increases in calcite and kaolinite could be related to a continued uplift of surrounding mountains exposing and reworking the older Paleogene sediment during the latest Miocene (Sun et al. 2008; Cao et al. 2013a).

Geochemical and isotopic data show a combined action of glacial and eolian activities in this time interval, with sediment sources from the western Kunlun Mountains, southern and northern flanks of the Tianshan Mountains, and soils from the Tibetan Plateau (Chang et al. 2000; Hattori et al. 2003; Honda and Shimizu 1998). The mineral composition of the Tarim Basin eolian sediment consists of Mg–Fe chlorite, amphibolite, and epidote, besides quartz, feldspar, and calcite (Chang et al. 2000). The sources of the eolian sediments in the Tarim Basin are thus likely basic and ultrabasic as well as felsic rock types from the surroundings of the Tarim Basin. These rocks transported by wind to the Tarim Basin are rich in Co, Cr, and Ni causing the increases in these elements with respect to UCC after 6.5 ± 0.5 Ma (Fig. 3), even though calcite contents increase causing lower Co/UCC, Cr/UCC, and Ni/UCC ratios (Parekh et al. 1977; Woolley and Kempe 1989). The slightly increased chlorite input could be from the eolian sources as well.

The eolian input and input from older Paleogene sediments can also account for the change of geochemical indices. The Ba/Sr and Rb/Sr ratios increasing after 6.5 ± 0.5 Ma can be explained by the observed increase in K-feldspar (Wang et al. 2013a; Zhang et al. 2002). The increases in kaolinite (CIA = 100), chlorite (CIA = 100), and smectite (CIA = 70–80) result in the increases in the CIA, PIA, CIW, and CIW′ indices. The decreased Na/Al ratio after 6.5 ± 0.5 Ma could be due to the increase in Al_2O_3 (Cao et al. 2014), which can be explained by the increase in Al-rich clays and K-feldspar as well as the decrease in plagioclase (Wang et al. 2013a). The decrease

in Na/Ti comes from an increase in TiO_2 probably mainly from rutile. Despite the fact that we do not detect rutile here, the sources of basic and ultrabasic as well as felsic rocks could well increase the rutile content, leading to the decrease in Na/Ti after 6.5 ± 0.5 Ma.

Implications for Tarim Basin climate and tectonics

We find climate cooling and drying after 17 Ma consistent with a negative shift of carbonate $\delta^{18}O$ in the Tarim Basin (Graham et al. 2005; Kent-Corson et al. 2009) and turnover of benthonic fauna (Hao et al. 1982a, b). The fossil genus *Ammonia* dominates in the Anjuan Formation, suggesting enhanced lake salinity (Hao et al. 1982a, b; Malmgren 1984). Also, *Cyprideis littoralis*, typical for brackish water, appears at the top of the Keziluoyi Formation. This species persists all the way through to the Pakabulake Formation, indicating lake water salinization (Jiang et al. 1995). The increased lake salinity can be the result of increased evaporation and/or decreased water supply due to climate cooling and drying.

The middle Miocene cooling and drying after 17 ± 1 Ma documented here postdates the major regional atmospheric reorganization in the late Oligocene to early Miocene during which the establishment of the modern East Asian monsoon is said to occur (Sun and Wang 2005; Guo et al. 2008). The cooling and drying trends are reversed to the observed trends in the northeastern Qinghai–Tibetan Plateau, where climates are warm during 17.1–14.7 Ma in the Tianshui Basin (Hui et al. 2011) and 18–14 Ma in the Qaidam Basin (Miao et al. 2011; Wang et al. 2013b), which are reported to be controlled by the global middle Miocene Climate Optimum (MCO). The global cooling at the middle Miocene Climate Transition could certainly have enhanced this cooling and drying since ~14 Ma, as the Na/Al, Na/Ti, CIA, PIA, CIW, and CIW′ proxies reach a peak at 14 ± 0.5 Ma. This intensified cooling and drying are also observed in the northeastern part of the QTP after 14.7 and 14 Ma in the Tianshui and Qaidam Basin, respectively (Miao et al. 2011; Hui et al. 2011). A different hydrological response could have taken place between continental interiors and continental margin sites at times of global warming during the MCO. An enhanced monsoon circulation could have caused increased rainfall in the Qaidam and Tianshui basins, while the Tarim Basin was too far from these atmospheric systems, and global warming caused drying. To further elaborate on this topic, it is important to more accurately date the Qimugan section.

The documented change of provenance at ~17 ± 1 Ma is broadly in line with exhumation records in the Pamir, West Kunlun, and Tianshan regions during the late Oligocene to middle Miocene (Amidon and Hynek 2010; Sobel and Dumitru 1997) and a substantial increase in accumulation rates at 16–17 Ma in the Kuche Depression (Huang et al. 2006), suggesting a phase of enhanced plateau uplift. In line with a tectonic origin of the observed Miocene shifts, detrital zircon age spectra show different age peaks before and after 17 Ma in our section (Cao et al. 2014). A sample before 17 Ma shows age peaks between 250–324 and 420–470 Ma, while a sample after 17 Ma shows age peaks at 20, 107, and 204 Ma. Climate change cannot cause such a dramatic shift of zircon age spectra. The ages in the Anjuan Formation indicate provenance in Miocene granites, Cretaceous granitoids, and Permain–Triassic gneisses and schists (Fig. 1a). The Pamir and West Kunlun ranges were apparently significantly activated in the basal parts of the middle Miocene Anjuan Formation, leading to a rapid exhumation of younger intrusive bodies and older gneisses and schists, explaining the 17 Ma increase in chlorite contents. This uplift could have diverted moisture-bearing westerlies and deepened aridity in the Tarim (Graham et al. 2005). Tectonic uplift could have caused drier climate trends in the west, while global climate caused wetter climates in the east.

The marine retreat from the Tarim Basin could not be the cause that triggered the cooling and drying here, even though Ritts et al. (2008) reported planktonic foraminifera from the base of the conglomeratic section to be Miocene in the east of the Tarim Basin. Firstly, the foraminifera were from conglomerates rather than from marine limestones, indicating that the microfossils were likely reworked by wind from upwind, more westerly regions. Secondly, most studies demonstrate that the last sea retreat from the Tarim Basin was at least before the Oligocene (Sun and Jiang 2013; Bosboom et al. 2011). In our section, there are no marine sediment layers in the Oligocene or Miocene (Bosboom et al. 2011). The Kezi section studied by Bosboom et al. 2011, in which they dated the last sea retreat as late Eocene, is approximately the same section as studied here. Thirdly, an integrated study along the southern Tarim from west to east (Hao et al. 1982a, b) did not reveal any marine microfossils in the Miocene.

A river channel shift causing the observed change at 17 ± 1 Ma seems unlikely, as the river would be expected to shift back at some point much quicker in time than the observed changes at million-year timescale. Besides, the above-mentioned reasons to, at least partially, relate the 17 Ma shift to tectonics, we note that the observed geochemical changes are not going along with the lithological changes that occur afterward.

Both tectonic uplift and initiated eolian input are responsible to the provenance change at ~6.5 Ma. Zircon and apatite fission-track chronological data have documented that the Kashgar–Yecheng transfer system was reactive during the latest Miocene 10–6 Ma (Cao et al. 2013a). This fault located near the south of the Qimugan section deforms

older Paleogene sediments, which were exposed and reworked producing the kaolinite and calcite re-deposition after 6.5 Ma. This deformation was observed at the nearby Sanju section as the strata angular unconformity at the latest Miocene (Sun et al. 2008). The eolian input is closely associated with the formation of Taklimakan Desert. Sun et al. (2009) and Sun and Liu (2006) have addressed this issue and pointed out that possibly both higher latitude cooling and ongoing regional tectonic uplift during the late Cenozoic are responsible for the formation of the Taklimakan Desert. This higher latitude cooling might have intensified the Siberian high pressure causing prevailing near-surface northeasterly winds in the Taklimakan Desert after this time. These eolian sediments cannot be blown out because of high relief of West Kunlun Mountains, but accumulate on the windward slopes of Kunlun Mountains mixed with the piedmont molasse deposits (Sun and Liu 2006).

Conclusions

Analysis of mineralogy, clay mineral morphology, major and minor elemental ratios, and chemical weathering indices in the southwestern part of the Tarim Basin shows two significant shifts in the earliest middle Miocene, at ~17 Ma, and in the latest Miocene, at ~6.5 Ma, respectively. The older is characterized by a decrease in Co, Cr, and Ni relative to UCC, in the chemical weathering indices (CIA, PIA, CIW and CIW′), and in Rb/Sr and Ba/Sr ratios, by increases in Na/Ti and Na/Al ratios, illite, smectite, and calcite contents, and changes of clay morphology from poorly developed lateral thickness, thin plates, and embayed edges to a thicker plates and rounded outlines. This step is interpreted as a combination of a provenance shift and regional climate cooling and drying. The decrease in Co/UCC, Cr/UCC, Ni/UCC, Rb/Sr, Ba/Sr, and illite as well as the increase in chlorite, smectite, and calcite, indicate that poorly weathered igneous and metamorphic rocks are the main sources in the Qimugan area between 17 ± 1 and 13.5 ± 0.5 Ma with additions of eroded Paleogene sediments. The decrease in CIA, PIA, CIW and CIW′ as well as increases in Na/Ti and Na/Al, however, suggest the climate cooling and drying after 17 ± 1 Ma. We conclude that the change of provenance here is a regional response of a phase of plateau uplift in line with earlier findings. The uplift of the mountains around the Tarim Basin possibly diverted moisture-bearing westerlies and triggered the climate cooling and drying since 17 ± 1 Ma.

A subsequent change occurred in the latest Miocene at 6.5 ± 0.5 Ma characterized by increases in Co, Cr, and Ni (relative to UCC), chemical weathering indices, Rb/Sr and Ba/Sr ratios, calcite, kaolinite, chlorite, and smectite contents, decreases in Na/Al and Na/Ti ratios, and illite content, and changes of clay morphology from rounded aggregates to thin plates with embayed edges. The clay morphology change showing characteristics of enhanced chemical weathering is not in line with the ongoing climate drying and cooling in this region. This points to enhanced input of chemically weathered material probably related to simultaneous onset of eolian dune building in the Tarim Basin. The sediment source after 6.5 ± 0.5 Ma is likely similar to that of the eolian dunes, which accumulate from the sources surrounding the Tarim Basin.

Acknowledgments We sincerely appreciate the editor in chief Wolf-Christian Dullo, the editor Prof. Wenjiao Xiao, Prof. Yuanbao Wu, Tiuri Konijnendijk, and three anonymous reviewers for their constructive comments and suggestions on earlier versions of this manuscript. We are grateful for grants from the Key Project Foundation of China Geological Survey (No. 1212011121261), the National Natural Science Foundation of China (Nos. 41072030 and 41272053), and the Independent Research Project Foundation of State Key Laboratory of Biogeology and Environmental Geology, China University of Geosciences, Wuhan (No. GKZ13Y657). C.W. acknowledges the Chinese Scholarship Council (CSC) for financial and Prof. Lucas J. Lourens for logistical support during his visit to Utrecht University.

References

Amidon WH, Hynek SA (2010) Exhumational history of the north central Pamir. Tectonics 29(TC5017):1–13. doi:10.1029/2009TC002589

An Z, Kutzbach JE, Prell WL, Porter SC (2001) Evolution of Asian monsoons and phased uplift of the Himalaya-Tibetan Plateau since late Miocene times. Nature 411(6833):62–66. doi:10.1038/35075035

Armentrout JM, Berta A (1977) Eocene-Oligocene foraminiferal sequence from the northeast Olympic Peninsula, Washington. J Foraminifer Res 7:216–233. doi:10.2113/gsjfr.7.3.216

Báldi K (2006) Paleoceanography and climate of the Badenian (Middle Miocene, 16.4–13.0 Ma) in the Central Paratethys based on foraminifera and stable isotope (δ18O and δ13C) evidence. Int J Earth Sci 95:119–142. doi:10.1007/s00531-005-0019-9

Blatt H, Sutherland B (1969) Intrastratal solution and non-opaque heavy minerals in shales. J Sediment Res 39:591–600. doi:10.1306/74D71CDA-2B21-11D7-8648000102C1865D

Blisniuk PM, Hacker BR, Glodny J, Ratschbacher L, Siwen B, Wu ZH, McWilliams MO, Calvert A (2001) Normal faulting in central Tibet since at least 13.5 Ma. Nature 412:628–632. doi:10.1038/35088045

Borges JB, Huh Y, Moon S, Noh H (2008) Provenance and weathering control on river bed sediments of the eastern Tibetan Plateau and the Russian Far East. Chem Geol 254:52–72. doi:10.1016/j.chemgeo.2008.06.002

Bosboom RE, Dupont-Nivet G, Houben AJP, Brinkhuis H, Villa G, Mandic O, Stoica M, Zachariasse WJ, Guo ZJ, Li CX (2011) Late Eocene sea retreat from the Tarim Basin (west China) and concomitant Asian paleoenvironmental change. Palaeogeogr Palaeoclimatol Palaeoecol 299:385–398. doi:10.1016/j.palaeo.2010.11.019

Bosboom RE, Dupont-Nivet G, Grothe A, Brinkhuis H, Villa G, Mandic O, Stoica M, Huang WT, Yang W, Guo ZJ, Krijgsman W (2013) Linking Tarim Basin sea retreat (west China) and Asian aridification in the late Eocene. Basin Res. doi:10.1111/bre.12054

Bougeois L, de Rafélis M, Reichart G, de Nooijer LJ, Nicollin F, Dupont-Nivet G (2014) A high resolution study of trace elements and stable isotopes in oyster shells to estimate Central Asian Middle Eocene seasonality. Chem Geol 363:200–212. doi:10.1016/j.chemgeo.2013.10.037

Buggle B, Glaser B, Hambach U, Gerasimenko N, Marković S (2011) An evaluation of geochemical weathering indices in loess - paleosol studies. Quat Int 240:12–21. doi:10.1016/j.quaint.2010.07.019

Cao K, Wang G, van der Beek P, Bernet M, Zhang K (2013a) Cenozoic thermo-tectonic evolution of the northeastern Pamir revealed by zircon and apatite fission-track thermochronology. Tectonophysics 589:17–32. doi:10.1016/j.tecto.2012.12.038

Cao K, Bernet M, Wang G, van der Beek P, Wang A, Zhang K, Enkelmann E (2013b) Focused Pliocene–Quaternary exhumation of the Eastern Pamir domes, western China. Earth Planet Sci Lett 363:16–26. doi:10.1016/j.epsl.2012.12.023

Cao K, Xu YD, Wang GC, Zhang KX, van der Beek P, Wang CW, Jiang SS, Bershaw J (2014) Neogene source-to-sink relations between the Pamir and Tarim Basin: insights from stratigraphy, detrital zircon geochronology, and whole-rock geochemistry. J Geol 122:433–454. doi:10.1086/676478

Chamley H (1989) Clay sedimentology. Springer, Berlin, Heidelberg, p 28

Chang Q, Mishima T, Yabuki S, Takahashi Y, Shimizu H (2000) Sr and Nd isotope ratios and REE abundances of moraines in the mountain areas surrounding the Taklimakan Desert, NW China. Geochem J 34:407–427

Chang H, An Z, Wu F, Jin Z, Liu W, Song Y (2013) A Rb/Sr record of the weathering response to environmental changes in westerly winds across the Tarim Basin in the late Miocene to the early Pleistocene. Palaeogeogr Palaeoclimatol Palaeoecol 386:364–373. doi:10.1016/j.palaeo.2013.06.006

Condie KC, Dengate J, Cullers RL (1995) Behavior of rare earth elements in a paleoweathering profile on granodiorite in the Front Range, Colorado, USA. Geochim Cosmochim Acta 59:279–294. doi:10.1016/0016-7037(94)00280-Y

DeCelles PG, Robinson DM, Zandt G (2002) Implications of shortening in the Himalayan fold-thrust belt for uplift of the Tibetan Plateau. Tectonics 21:6–1062. doi:10.1029/2001TC001322

Dettman DL, Fang X, Garzione CN, Li J (2003) Uplift-driven climate change at 12 Ma: a long δ18O record from the NE margin of the Tibetan plateau. Earth Planet Sci Lett 214:267–277. doi:10.1016/S0012-821X(03)00383-2

Dong X, Ding Z, Yang S, Luo P, Wang X, Ji J (2013) Synchronous drying and cooling in central Asia during late Oligocene. Chin Sci Bull 58(25):3119–3124. doi:10.1007/s11434-013-5821-3

Drits VA, Sakharov BA, Dainyak LG, Salyn AL, Lindgreen H (2002) Structural and chemical heterogeneity of illite-smectites from Upper Jurassic mudstones of East Greenland related to volcanic and weathered parent rocks. Am Miner 87:1590–1607

Dupont-Nivet G, Hoorn C, Konert M (2008) Tibetan uplift prior to the Eocene-Oligocene climate transition: evidence from pollen analysis of the Xining Basin. Geology 36:987–990. doi:10.1130/G25063A.1

Fang XM, Zhang WL, Meng QQ, Gao JP, Wang XM, King J (2007) High-resolution magnetostratigraphy of the Neogene Huaitoutala section in the eastern Qaidam Basin on the NE Tibetan Plateau, Qinghai Province, China and its implication on tectonic uplift of the NE Tibetan Plateau. Earth Planet Sci Lett 258:293–306. doi:10.1016/j.epsl.2007.03.042

Fedo CM, Nesbitt HW, Young GM (1995) Unraveling the effects of potassium metasomatism in sedimentary rocks and paleosols, with implications for paleoweathering conditions and provenance. Geology 23:921–924. doi:10.1130/0091-7613(1995)023<0921:UTEOPM>2.3.CO;2

Fralick PW, Kronberg BI (1997) Geochemical discrimination of clastic sedimentary rock sources. Sed Geol 113:111–124. doi:10.1016/S0037-0738(97)00049-3

Gebhardt H (2003) Palaeobiogeography of Late Oligocene to Early Miocene Central European Ostracoda and Foraminifera: progressive isolation of the Mainz Basin, northern Upper Rhine Graben and Hanau Basin/Wetterau. Palaeogeogr Palaeoclimatol Palaeoecol 201:343–354. doi:10.1016/S0031-0182(03)00619-9

Graham SA, Chamberlain CP, Yue Y, Ritts BD, Hanson AD, Horton TW, Waldbauer JR, Poage MA, Feng X (2005) Stable isotope records of Cenozoic climate and topography, Tibetan Plateau and Tarim Basin. Am J Sci 305:101–118. doi:10.2475/ajs.305.2.101

Guo ZT, Ruddiman WF, Hao QZ, Wu HB, Qiao YS, Zhu RX, Peng SZ, Wei JJ, Yuan BY, Liu TS (2002) Onset of Asian desertification by 22 Myr ago inferred from loess deposits in China. Nature 416:159–163. doi:10.1038/416159a

Guo ZT, Sun B, Zhang ZS, Peng SZ, Xiao GQ, Ge JY, Hao QZ, Qiao YS, Liang MY, Liu JF (2008) A major reorganization of Asian climate by the early Miocene. Clim Past 4:153–174. doi:10.5194/cp-4-153-2008

Hao YC, Zeng XL, Qiu SY, He XX (1982a) Miocene foraminifera of Tarim basin, Xinjiang and their geological significance. Bull Chin Acad Geol Sci 4:69–79

Hao YC, Zeng XL, Li HM (1982b) Late Cretaceous and Tertiary strata and foraminifera in west Talimu Basin. Earth Sci J Wuhan Coll Geol 17:1–186 **(In Chinese with English abstract)**

Harnois L (1988) The CIW index: a new chemical index of weathering. Sed Geol 55:319–322. doi:10.1016/0037-0738(88)90137-6

Harrison T, Copeland P, Kidd WSF, Yin A (1992) Raising tibet. Science 255:1663–1670. doi:10.1126/science.255.5052.1663

Hattori Y, Suzuki K, Honda M, Shimizu H (2003) Re-Os isotope systematics of the Taklimakan Desert sands, moraines and river sediments around the Taklimakan Desert, and of Tibetan soils. Geochim Cosmochim Acta 67:1203–1213. doi:10.1016/S0016-7037(02)01206-1

Heermance RV, Chen J, Burbank DW, Miao J (2008) Temporal constraints and pulsed Late Cenozoic deformation during the structural disruption of the active Kashi foreland, northwest China. Tectonics. doi:10.1029/2007TC002226

Honda M, Shimizu H (1998) Geochemical, mineralogical and sedimentological studies on the Taklimakan Desert sands. Sedimentology 45:1125–1143. doi:10.1046/j.1365-3091.1998.00202.x

Hong HL, Li ZH, Xue HJ, Zhu YH, Zhang KX, Xiang SY (2007) Oligocene clay mineralogy of the Linxia Basin: evidence of Paleoclimatic evolution subsequent to the initial-stage uplift of the Tibetan Plateau. Clays Clay Miner 55:492–505. doi:10.1346/CCMN.2007.0550504

Hong HL, Zhang KX, Li ZH (2010) Climatic and tectonic uplift evolution since ~7 Ma in Gyirong basin, southwestern Tibet plateau: clay mineral evidence. Int J Earth Sci 99:1305–1315. doi:10.1007/s00531-009-0457-x

Hong HL, Wang CW, Zeng KF, Zhang KX, Yin K, Li ZH (2012) Clay mineralogy of the Zhada sediments: evidence for climatic and tectonic evolution since ~9 Ma in Zhada, southwestern Tibet. Clays Clay Miner 60:240–253. doi:10.1346/CCMN.2012.0600302

Huang B, Piper JDA, Peng S, Liu T, Li Z, Wang Q, Zhu R (2006) Magnetostratigraphic study of the Kuche Depression, Tarim Basin, and Cenozoic uplift of the Tian Shan range, western China. Earth Planet Sci Lett 251:346–364. doi:10.1016/j.epsl.2006.09.020

Hui Z, Li J, Xu Q, Song C, Zhang J, Wu F, Zhao Z (2011) Miocene vegetation and climatic changes reconstructed from a sporopollen record of the Tianshui Basin, NE Tibetan Plateau. Palaeogeogr Palaeoclimatol Palaeoecol 308(3):373–382. doi:10.1016/j.palaeo.2011.05.043

Hurlbut CS, Klein C (1985) Manual of mineralogy. Wiley, New York, p 324

International Commission on Stratigraphy (2015) http://www.stratigraphy.org/ICSchart/ChronostratChart-2015-01.pdf

Ji J, Luo P, White P, Jiang H, Gao L, Ding Z (2008) Episodic uplift of the Tianshan Mountains since the late Oligocene constrained by magnetostratigraphy of the Jingou River section, in the southern margin of the Junggar Basin, China. J Geophys Res 113:B05102. doi:10.1029/2007JB005064

Ji JL, Zhang KX, Qiang T, Kou XH, Chen FL, Xu YD, Lu JF, Lin Q (2010) Magnetostratigraphy of the Neogene Strata in Xunhua Basin, Qinghai Province. Earth Sci 35:803–810 **(In Chinese with Englsih Abstract)**

Jiang XT, Zhou WF, Lin S (1995) Stratigraphy and Ostracods of Xinjiang in China. Geological Publishing House, Beijin **(In Chinese)**

Jin X, Wang J, Chen B, Ren L (2003) Cenozoic depositional sequences in the piedmont of the west Kunlun and their paleogeographic and tectonic implications. J Asian Earth Sci 21:755–765. doi:10.1016/S1367-9120(02)00073-1

Jolivet M, Brunel M, Seward D, Xu Z, Yang J, Roger F, Tapponnier P, Malavieille J, Leyreloup A, Arnaud N, Wu C (2001) Mesozoic and Cenozoic tectonics of the northern edge of the Tibetan plateau: fission-track constraints. Tectonophysics 343:111–134. doi:10.1016/S0040-1951(01)00196-2

Jolivet M, Brunel M, Seward D, Xu Z, Yang J, Malavieille J, Roger F, Leyreloup A, Arnaud N, Wu C (2003) Neogene extension and volcanism in the Kunlun Fault Zone, northern Tibet: new constraints on the age of the Kunlun Fault. Tectonics. doi:10.1029/2002TC001428

Kent-Corson ML, Ritts BD, Zhuang G, Bovet PM, Graham SA, Page Chamberlain C (2009) Stable isotopic constraints on the tectonic, topographic, and climatic evolution of the northern margin of the Tibetan Plateau. Earth Planet Sci Lett 282(1):158–166. doi:10.1016/j.epsl.2009.03.011

Li Z, Peng S (2010) Detrital zircon geochronology and its provenance implications: responses to Jurassic through Neogene basin-range interactions along northern margin of the Tarim Basin, Northwest China. Basin Res 22:126–138. doi:10.1111/j.1365-2117.2009.00440.x

Ligios S, Benvenuti M, Gliozzi E, Papini M, Rook L (2008) Late Miocene palaeoenvironmental evolution of the Baccinello-Cinigiano Basin (Tuscany, central Italy) and new autoecological data on rare fossil fresh-to brackish-water ostracods. Palaeogeogr Palaeoclimatol Palaeoecol 264:277–287. doi:10.1016/j.palaeo.2007.04.018

Lu HJ, Xiong SF (2009) Magnetostratigraphy of the Dahonggou section, northern Qaidam Basin and its bearing on Cenozoic tectonic evolution of the Qilian Shan and Altyn Tagh Fault. Earth Planet Sci Lett 288:539–550. doi:10.1016/j.epsl.2009.10.016

Lukens CE, Carrapa B, Singer BS, Gehrels G (2012) Miocene exhumation of the Pamir revealed by detrital geothermochronology of Tajik rivers. Tectonics. doi:10.1029/2011TC003040

Luo MS, Lü XL, Zhang KX, Chen FL, Xu YD, Chen RM, Song BW (2010) Middle Miocene-Early Pliocene ostracod assemblages in the Xunhua Basin, Qinghai and their geological significance. Acta Micropalaeontol Sin 27(2):125–134 **(In Chinese with English Abstract)**

Malmgren BA (1984) Analysis of the environmental influence on the morphology of Ammonia beccarii (Linné) in southern European salinas. Geobios 17:737–746. doi:10.1016/S0016-6995(84)80118-7

Malusà MG, Zattin M, Andò S, Garzanti E, Vezzoli G (2009) Focused erosion in the Alps constrained by fission-track ages on detrital apatites. Geol Soc Lond Spec Publ 324:141–152. doi:10.1144/SP324.11

McLennan SM (1993) Weathering and global denudation. J Geol 101:295–303

McLennan SM (2001) Relationships between the trace element composition of sedimentary rocks and upper continental crust. Geochem Geophys Geosyst 2:2009G–2109G. doi:10.1029/2000GC000109

Métivier F, Gaudemer Y, Tapponnier P, Meyer B (1998) Northeastward growth of the Tibet plateau deduced from balanced reconstruction of two depositional areas: the Qaidam and Hexi Corridor basins, China. Tectonics 17:823–842. doi:10.1029/98TC02764

Miao Y, Fang X, Herrmann M, Wu F, Zhang Y, Liu D (2011) Miocene pollen record of KC-1 core in the Qaidam Basin, NE Tibetan Plateau and implications for evolution of the East Asian monsoon. Palaeogeogr Palaeoclimatol Palaeoecol 299:30–38. doi:10.1016/j.palaeo.2010.10.026

Molnar P, Tapponnier P (1975) Cenozoic tectonics of Asia: effects of a continental collision. Science 189:419–426

Molnar P, England P, Joseph M (1993) Mantle dynamics, uplift of the Tibetan plateau, and the Indian monsoon. Rev Geophys 31:357–396. doi:10.1029/93RG02030

Molnar P, Boos WR, Battisti DS (2010) Orographic controls on climate and paleoclimate of Asia: thermal and mechanical roles for the Tibetan Plateau. Ann Rev Earth Planet Sci 38:77–102. doi:10.1146/annurev-earth-040809-152456

Nesbitt HW, Markovics G (1980) Chemical processes affecting alkalis and alkaline earths during continental weathering. Geochim Cosmochim Acta 44:1659–1666. doi:10.1016/0016-7037(80)90218-5

Nesbitt HW, Young GM (1982) Early Proterozoic climates and plate motions inferred from major element chemistry of lutites. Nature 299:715–717. doi:10.1038/299715a0

Paillard D, Labeyrie L, Yiou P (1996) Macintosh program performs time-series analysis. Eos Trans Am Geophys Union 77:379. doi:10.1029/96EO00259

Parekh PP, Möller P, Dulski P, Bausch WM (1977) Distribution of trace elements between carbonate and non-carbonate phases of limestone. Earth Planet Sci Lett 34:39–50. doi:10.1016/0012-821X(77)90103-0

Perry EA, Hower J (1970) Burial diagenesis in Gulf Coast politic sediments. Clays Clay Miner 18:165–177. doi:10.1346/CCMN.1970.0180306

Ramstein G, Fluteau F, Besse J, Joussaume S (1997) Effect of orogeny, plate motion and land-sea distribution on Eurasian climate change over the past 30 million years. Nature 386:788–795. doi:10.1038/386788a0

Rieser AB, Bojar AV, Neubauer F, Genser J, Liu Y, Ge XH, Friedl G (2009) Monitoring Cenozoic climate evolution of northeastern Tibet: stable isotope constraints from the western Qaidam Basin, China. Int J Earth Sci 98:1063–1075. doi:10.1007/s00531-008-0304-5

Ritts BD, Yue YJ, Graham S, Sobel ER, Abbink OA, Stockli D (2008) From sea level to high elevation in 15 million years: uplift history of the northern Tibetan Plateau margin in the Altun Shan. Am J Sci 308:657–678. doi:10.2475/05.2008.01

Robert C, Kennett JP (1997) Antarctic continental weathering changes during Eocene–Oligocene cryosphere expansion: clay mineral and oxygen isotope evidence. Geology 25:587–590. doi:10.1130/0091-7613(1997)025<0587:ACWCDE>2.3.CO;2

Robinson AC, Yin A, Manning CE, Harrison TM, Zhang SH, Wang XF (2004) Tectonic evolution of the northeastern Pamir: constraints from the northern portion of the Cenozoic Kongur Shan extensional system, western China. Geol Soc Am Bull 116:953–973. doi:10.1130/B25375.1

Robinson AC, Yin A, Manning CE, Harrison TM, Zhang SH, Wang XF (2007) Cenozoic evolution of the eastern Pamir:

implications for strain-accommodation mechanisms at the western end of the Himalayan-Tibetan orogen. Geol Soc Am Bull 119:882–896. doi:10.1130/B25981.1

Sobel ER, Dumitru TA (1997) Thrusting and exhumation around the margins of the western Tarim basin during the India-Asia collision. J Geophys Res 102:5043–5063. doi:10.1029/96JB03267

Sobel ER, Chen J, Heermance RV (2006) Late Oligocene-Early Miocene initiation of shortening in the Southwestern Chinese Tian Shan: implications for Neogene shortening rate variations. Earth Planet Sci Lett 247:70–81. doi:10.1016/j.epsl.2006.03.048

Sun J, Jiang M (2013) Eocene seawater retreat from the southwest Tarim Basin and implications for early Cenozoic tectonic evolution in the Pamir Plateau. Tectonophysics 588:27–38. doi:10.1016/j.tecto.2012.11.031

Sun J, Liu T (2006) The age of the Taklimakan Desert. Science 312:1621. doi:10.1126/science.1124616

Sun X, Wang P (2005) How old is the Asian monsoon system? Palaeobotanical records from China. Palaeogeogr Palaeoclimatol Palaeoecol 222:181–222. doi:10.1016/j.palaeo.2005.03.005

Sun Z, Feng X, Li D, Yang F, Qu Y, Wang H (1999) Cenozoic Ostracoda and palaeoenvironments of the northeastern Tarim Basin, western China. Palaeogeogr Palaeoclimatol Palaeoecol 148:37–50. doi:10.1016/S0031-0182(98)00174-6

Sun J, Zhu R, An Z (2005a) Tectonic uplift in the northern Tibetan Plateau since 13.7 Ma ago inferred from molasse deposits along the Altyn Tagh Fault. Earth Planet Sci Lett 235:641–653. doi:10.1016/j.epsl.2005.04.034

Sun Z, Yang Z, Pei J, Ge X, Wang X, Yang T, Li W, Yuan S (2005b) Magnetostratigraphy of Paleogene sediments from northern Qaidam Basin, China: implications for tectonic uplift and block rotation in northern Tibetan plateau. Earth Planet Sci Lett 237:635–646. doi:10.1016/j.epsl.2005.07.007

Sun J, Zhang L, Deng C, Zhu R (2008) Evidence for enhanced aridity in the Tarim Basin of China since 5.3 Ma. Quat Sci Rev 27:1012–1023

Sun J, Zhang Z, Zhang L (2009) New evidence on the age of the Taklimakan Desert. Geology 37:159–162. doi:10.1130/G25338A.1

Sun J, Gong ZJ, Tian ZH, Jia YY, Windley B (2015) Late Miocene stepwise aridification in the Asian interior and the interplay between tectonics and climate. Palaeogeogr Palaeoclimatol Palaeoecol 421:48–59. doi:10.1016/j.palaeo.2015.01.001

Vanderaveroet P (2000) Miocene to Pleistocene clay mineral sedimentation on the New Jersey shelf. Oceanol Acta 23:25–36. doi:10.1016/S0399-1784(00)00102-X

Wang D, Sun X, Zhao Y (1990) Late Cretaceous to Tertiary palynofloras in Xinjiang and Qinghai, China. Rev Palaeobot Palynol 65:95–104. doi:10.1016/0034-6667(90)90060-V

Wang E, Wan J, Liu J (2003a) Late Cenozoic geological evolution of the foreland basin bordering the West Kunlun range in Pulu area: constraints on timing of uplift of northern margin of the Tibetan Plateau. J Geophys Res 108(B8):2401. doi:10.1029/2002JB001877

Wang X, Wang B, Qiu Z, Xie G, Xie J, Downs W, Qiu Z, Deng T (2003b) Danghe area (western Gansu, China) biostratigraphy and implications for depositional history and tectonics of northern Tibetan Plateau. Earth Planet Sci Lett 208:253–269

Wang GC, Cao K, Zhang KX, Wang A, Liu C, Meng YN, Xu YD (2011) Spatio-temporal framework of tectonic uplift stages of the Tibetan Plateau in Cenozoic. Sci Chin Earth Sci 54:29–44. doi:10.1007/s11430-010-4110-0

Wang C, Hong HL, Li ZH, Yin K, Xie J, Liang GJ, Song BW, Song EP, Zhang KX (2013a) The Eocene–Oligocene climate transition in the Tarim Basin, Northwest China: evidence from clay mineralogy. Appl Clay Sci 74:10–19. doi:10.1016/j.clay.2012.09.003

Wang C, Hong HL, Li ZH, Liang GJ, Xie J, Song BW, Song EP, Zhang KX (2013b) Climatic and tectonic evolution in the Qaidam since the Cenozoic: evidence from sedimentology and mineralogy. J Earth Sci 24:314–327. doi:10.1007/s12583-013-0332-3

Warr LN, Rice A (1994) Interlaboratory standardization and calibration of day mineral crystallinity and crystallite size data. J Metamorph Geol 12:141–152. doi:10.1111/j.1525-1314.1994.tb00010.x

Winkler A, Wolf-Welling T, Stattegger K, Thiede J (2002) Clay mineral sedimentation in high northern latitude deep-sea basins since the Middle Miocene (ODP Leg 151, NAAG). Int J Earth Sci 91:133–148. doi:10.1007/s005310100199

Woolley AR, Kempe DRC (1989) Carbonatites: nomenclature, average chemical compositions, and element distribution. In: Bell K (ed) Carbonatites: genesis and evolution. Unwin Hyman, London

Xiao GQ, Abels HA, Yao QZ, Dupont-Nivet G, Hilgen FJ (2010) Asian aridification linked to the first step of the Eocene-Oligocene climate Transition (EOT) in obliquity-dominated terrestrial records (Xining Basin, China). Clim Past 6:501–513. doi:10.5194/cp-6-501-2010

Yin A, Harrison TM (2000) Geologic evolution of the Himalayan-Tibetan orogen. Ann Rev Earth Planet Sci 28:211–280. doi:10.1146/annurev.earth.28.1.211

Yin A, Rumelhart PE, Butler R, Cowgill E, Harrison TM, Foster DA, Ingersoll RV, Qing Z, Zhou X, Wang X, Lanson A, Raza A (2002) Tectonic history of the Altyn Tagh fault system in northern Tibet inferred from Cenozoic sedimentation. Geol Soc Am Bull 114:1257–1295. doi:10.1130/0016-7606(2002)114<1257:THOTAT>2.0.CO;2

Yue Y, Liou JG (1999) Two-stage evolution model for the Altyn Tagh fault, China. Geology 27:227. doi:10.1130/0091-7613(1999)027<0227:TSEMFT>2.3.CO;2

Zhang C, Wang L, Li G, Dong S, Yang J, Wang X (2002) Grain size effect on multi-element concentrations in sediments from the intertidal flats of Bohai Bay, China. Appl Geochem 17:59–68. doi:10.1016/S0883-2927(01)00079-8

Zhang KX, Wang GC, Ji JL, Luo MS, Kou XH, Wang YM, Xu YD, Chen FN, Chen RM, Song BW (2010) Paleogene-Neogene stratigraphic realm and sedimentary sequence of the Qinghai-Tibet Plateau and their response to uplift of the plateau. Sci Chin Earth Sci 53:1271–1294. doi:10.1007/s11430-010-4048-2

Zhang Z, Han W, Fang X, Song C, Li X (2013) Late Miocene-Pleistocene aridification of Asian inland revealed by geochemical records of lacustrine-fan delta sediments from the western Tarim Basin, NW China. Palaeogeogr Palaeoclimatol Palaeoecol 377:52–61. doi:10.1016/j.palaeo.2013.03.008

Zheng H, Powell CMA, An Z, Zhou J, Dong G (2000) Pliocene uplift of the northern Tibetan Plateau. Geology 28:715–718. doi:10.1130/0091-7613(2000)28<715:PUOTNT>2.0.CO;2

Zheng H, Tada R, Jia J, Lawrence C, Wang K (2010) Cenozoic sediments in the southern Tarim Basin: implications for the uplift of northern Tibet and evolution of the Taklimakan Desert. Geol Soc Lond Spec Publ 342:67–78. doi:10.1144/SP342.6